Enhancing Quantum Metrology with High-order Fisher Information and Experiments

Xin-Zhu Liu[1], Jun-Li Jiang[1], Yan-Han Yang[1], Li-Ming Zhao[1], Xue Yang[1], Shao-Ming Fei[2] and Ming-Xing Luo[1,3†]

1 School of Information Science and Technology, Southwest Jiaotong University, Chengdu 610031, China
2 Max-Planck-Institute for Mathematics in the Sciences, 04103 Leipzig, Germany
3 Hefei National Laboratory, University of Science and Technology of China, Hefei, Anhui 230088, China

† mxluo@swjtu.edu.cn

Abstract

Fisher information plays a central role in statistics and quantum metrology, providing the basis for the celebrated Cramér-Rao bound. In this work, we introduce a new information measure based on higher-order Fisher information and show that it naturally leads to a generalized uncertainty relation for parameter estimation, which can be regarded as an extension of the Cramér-Rao bound. As an application, we analyze the case of quantum phase estimation with a single qubit and compare our theoretical bounds with the well-known established hierarchical bounds. Finally, we experimentally validate the proposed framework using a photonic platform.

Copyright attribution to authors.
This work is a submission to SciPost Physics.
License information to appear upon publication.
Publication information to appear upon publication.

Received Date
Accepted Date
Published Date

Contents

1 Introduction

The Cramér-Rao bound (CRB) evaluates estimator performance via Fisher Information (FI) [1, 2]. Helstrom extended this to the quantum domain by replacing probability functions with density operators [3], leading to the quantum Cramér-Rao inequality, a quantized version of the classical bound optimized over all quantum measurements [4]. This introduced quantum Fisher information(QFI), quantifying information encoded in quantum states. Various extensions such as multiparameter estimation [5], adaptive Bayesian methods [6], and photonic implementations surpassing the Heisenberg limit [7] highlight quantum technologies' potential for precision measurements in applications like gravitational wave detection and biosensing [8–18, 18–21].

The standard estimation error in quantum metrology depends on QFI, which relies solely on the first-order derivative of the spherical representation of statistical distributions. This limits its ability to characterize parameters because of its specific regularity conditions optimally. Recent advancements have addressed this by generalizing quantum metrology through the Bures metric and linear combinations of general test functions, enabling the quantization of various well-known bounds [22]. These methods create hierarchies of frequentist bounds [22–27], including the QCRB. Such developments provide a more comprehensive framework for parameter estimation, particularly in scenarios where the QCRB falls short.

In this paper, we propose a generalized form of information derived from FI. This information can be treated as a score function, and it corresponds to the higher-order derivative of the spherical representation of estimated probability distributions (see Figure 1). This information naturally leads to a generalized uncertainty relation for metrology. We apply this framework to quantum phase estimation with a single qubit, deriving an improved theoretical bound. We compare it with well-established hierarchical bounds, including QCRB [3,23,24,27], quantum Bhattacharyya bounds [26], quantum Abel bounds [25], and Gessner-Smerzi bounds [22]. Finally, we validate our method experimentally using a photonic platform, demonstrating its practical applicability. Despite the non-additive feature of the present high-order information, our bound demonstrates asymptotic properties, and the estimation error can be minimized with multiple measurements. We experimentally validate a quantum phase estimation using a single-photon platform.

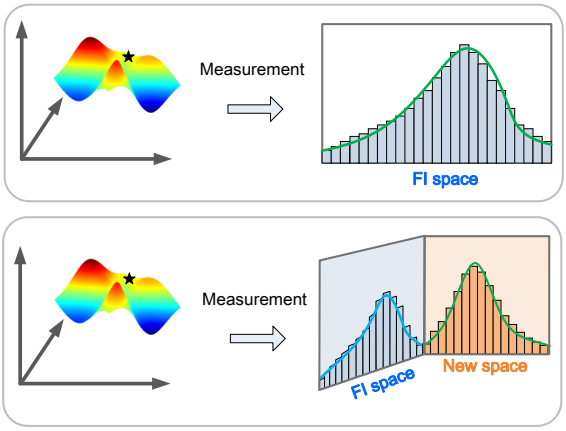

Figure 1: Schematic metrology using Fisher information (up) and both Fisher information and present high-order information (down). The estimation errors of parameterized unknown variables can be characterized in terms of different feature spaces defined by Fisher information and second-order information.

2 Metrology with high-order information

Consider a statistical experiment designed to infer an unknown parameter θ, where $\{p(x|\theta) : \theta \in \Theta\}$ represents a family of probability densities for a continuous random variable X on $\mathbb{D} \subseteq \mathbb{R}$. For an unbiased estimator $\hat{\theta}$, i.e., $\langle\hat{\theta}\rangle_{\theta_0} = \theta_0$ for all $\theta_0 \in \Theta$, the estimation error is characterized by using the variance of the estimator given by: $\Delta\hat{\theta}^2 = \int p(x|\theta)(\hat{\theta} - \langle\hat{\theta}\rangle_\theta)^2 dx$, where $\langle\hat{\theta}\rangle_\theta = \int p(x|\theta)\hat{\theta}(x)dx$. The classical metrology mainly depends on the Cramér-Rao inequality that relates the estimation error to the so-called FI [1, 2], which is defined as $I = 4\int(\partial_\theta\sqrt{p(x|\theta)})^2 dx$. Here, FI measures the sensitivity of the probability density $p(x|\theta)$ to the changes in the parameter θ. As FI depends only on the first-order derivative of the likelihood function, the standard CRB relies on certain regularity conditions [1, 2]. This limits its applications especially for one-copy scenarios.

To address this problem, we extend the parameter estimation framework to incorporate higher-order derivatives of the likelihood function, enabling a more comprehensive analysis of parameter estimation in statistical experiments. Specifically, we use the second-order derivative of the likelihood function, leading to a new measure of information as

$$I_2 \equiv 4\int(\partial_\theta^2\sqrt{p(x|\theta)})^2 dx \tag{1}$$

In the special case of $\partial_\theta \log p(x|\theta) = 0$, the present information of definition (1) corresponds to the second moment of the second derivative of the log-likelihood function at the true value. In contrast, the standard FI corresponds to the negative expectation of the second derivative. Rewriting the form of I_2 as $I_2 = \int p(x|\theta)\left[\partial_\theta^2 \ln p(x|\theta)) + \frac{1}{2}(\partial_\theta \ln p(x|\theta))^2\right]^2 dx$. This shows that second-order information captures both the first- and second-order sensitivities of the log-likelihood function, providing a more nuanced measure of the parameter sensitivity.

Now, we apply the present second-order information to characterize the estimation error. Given an unbiased estimator $\hat{\theta}$ of the unknown parameter θ, we show that the variance of estimation error is bounded from below as follows (See Appendix A):

$$\Delta\hat{\theta}^2 \geq \frac{4\mathbb{E}_I^2}{I_2} \tag{2}$$

where $\mathbb{E}_I = \int (\hat{\theta}-\theta)(\partial_\theta \sqrt{p_\theta(x)})^2 dx$. For the point estimation, the bound can be sharpened to $\Delta\hat{\theta}^2 \geq (\theta - \|\hat{\theta}\|_2)^2 \frac{I^2}{4I_2}$, where $\|\hat{\theta}\|_2^2 = \int \hat{\theta}^2 dx$.

The uncertainty relationship of (2) generalizes the CRB by combining the first- and second-order estimators, offering a more robust framework for parameter estimation in scenarios where higher-order sensitivities are relevant [28–30].

3 Quantum metrology with high-order information

Given a parameterized density matrix ρ_θ, we extend the high-order information (1) into quantum scenario as:

$$I_2^q = 4\,\mathrm{Tr}\left(\partial_\theta^2 \sqrt{\rho_\theta}\right)^2 \tag{3}$$

In the quantum scenario, the probability function is replaced by a density matrix for the quantum state. This new quantity I_2^q incorporates the higher-order sensitivities of the quantum state with respect to the parameter θ. It can be evaluated using the spectral decomposition of the density operator ρ_θ and the symmetric logarithmic derivative (SLD) formalism [4] (See Appendix C). This extension provides a more detailed characterization of parameter sensitivity in quantum systems, complementing the standard QFI.

So far, most of the results in quantum metrology reply on the quantum extensions of FI [3, 31], defined as QFI: $I^q = 4\,\mathrm{Tr}\left(\frac{\partial\sqrt{\rho_\theta}}{\partial\theta}\right)^2$. In the following, we improve the quantum metrology by generalizing the classical high-order information framework to quantum systems.

In the case of parameter estimation, consider an estimation operator $M := \sum_x h(x)\, E_x$ including positive operator-valued measure (POVM) $\{E_x\}$ and an estimation function $h : \mathcal{X} \to \mathbb{R}$. The unbiasedness assumption means $\mathrm{Tr}(M\rho_\theta) = \sum_x h(x)\,\mathrm{Tr}(\rho_\theta E_x) = \theta$. We quantify the measurement error by using the mean-squared error defined by $\Delta M^2 := \mathrm{Var}(\hat{\theta})$ $= \mathrm{Tr}(M^2\rho_\theta) - [\mathrm{Tr}(M\rho_\theta)]^2$. The optimal performance of measurement and classical post-processing is then defined via

$$\mathrm{Var}_\theta^\star := \inf_{\{E_x\},\, h} \left\{ \mathrm{Tr}\big(M^2\rho_\theta\big) - \big[\mathrm{Tr}(M\rho_\theta)\big]^2 \right\} \tag{4}$$

which should be subject to the unbiasedness assumption.

By incorporating the high-order correlation (3), we show that the variance of the quantum estimator M can be bounded by:

$$\Delta M^2 \geq \frac{4\mathbb{E}_{I^q}^2}{I_2^q} \tag{5}$$

where $\mathbb{E}_{I^q}$ is defined by $\mathbb{E}_{I^q} = \mathrm{Tr}((M-\theta)(\partial_\theta\sqrt{\rho_\theta})^2)$. The asymptotically saturable condition of this inequality implies that a non-normal distribution different from the normal distribution of QCRB, see Appendix A.2.

4 Thermodynamic metrology with high-order information

Thermodynamic constraints provide a natural setting to investigate the fundamental limits of quantum systems, where coherence plays a central role in determining performance and resource costs [21, 32, 33]. In this context, we explore how high-order information can be employed to analyze thermodynamical parameter estimations.

Consider a thermal state $\rho = \frac{1}{Z}e^{-\beta H}$, where $\beta = \frac{1}{k_B T}$ is the inverse temperature (with Boltzmann constant k_B), and $Z = \mathrm{Tr}e^{-\beta H}$ is the partition function. The main goal is to estimate the temperature that generally involves the heat capacity C_v, defined as: $C_v = \partial_T \langle H \rangle = \frac{\Delta H^2}{T^2}$, where ΔH^2 denotes the variance of the Hamiltonian, and $k_B = 1$ [34, 35]. Note the QFI for temperature estimation is directly proportional to the specific heat: $I^q = \frac{1}{T^4}\Delta H^2 = \frac{1}{T^2}C_v$ [34, 35]. Suppose the Hamiltonian H is an unbiased measurement for extracting the temperature of a given thermal state. By applying the definition of the second-order information (3) and the inequality (5), we show a new relation of the heat capacity and high-order information as

$$C_v^3 \geq \frac{|T - \|H\|_F|^2}{4T^6 I_2^q} \tag{6}$$

This result enhances understanding of how quantum systems dissipate or retain energy under thermal fluctuations by correlating the quantum information with thermodynamic properties.

Now, we show the inequality (10). For a thermal state, we have $e^{-\frac{1}{T}H} = Z\rho$, $\partial_T e^{-\frac{1}{T}H} = \frac{H}{T^2}Z\rho$, and $\partial_T \mathrm{Tr}e^{-\frac{1}{T}H} = \frac{Z}{T^2}\langle H \rangle$. This implies that

$$\begin{aligned} \partial_T \rho &= -\frac{1}{Z^2}\partial_T(\mathrm{Tr}e^{-\frac{1}{T}H})e^{-\frac{1}{T}H} + \frac{1}{Z}\frac{H}{T^2}e^{-\frac{1}{T}H} \\ &= \frac{1}{T^2}(H - \langle H \rangle)\rho \end{aligned} \tag{7}$$

where $\langle H \rangle$ denotes the expect of the Hamiltonian H with respect to the thermal state, i.e., $\langle H \rangle = \mathrm{Tr}(H\rho)$. The heat capacity [21, 36] is then given by

$$C_v = \partial_T \langle H \rangle = \frac{1}{T^2}\Delta H^2$$

where ΔH^2 denotes the variance of the Hamiltonian and $\langle H^k \rangle$ denotes the expect of the operator H^k with respect to the thermal state, i.e., $\langle H^k \rangle = \mathrm{Tr}(H^k\rho)$.

By taking the second derivative of ρ with respect to the temperature T, it follows that

$$\partial_T^2 \rho = \frac{1}{T^4}(\hat{H}^2 - \Delta H^2)\rho - \frac{2}{T^3}\hat{H}\rho \tag{8}$$

with $\hat{H} = H - \langle H \rangle$. Since the Hamiltonian H of the defined thermal state is temperature-independent, H and ρ are commutative. The second-order quantum information can be written as

$$I_2^q = \frac{1}{4T^8}\Delta H^4 - \frac{2}{T^7}\Delta H^3 + \frac{4}{T^6}\Delta H^2 \tag{9}$$

where $\Delta H^k = \mathrm{Tr}(\rho \hat{H}^k)$.

Finally, suppose the Hamiltonian H defines an unbiased measurement for extracting the temperature of a given thermal state. The second-order quantum information, alongside temperature and heat capacity, satisfies the following inequality

$$C_v^3 \geq \frac{|T - \|H\|_F|^2}{4T^6 I_2^q} \tag{10}$$

This shows how quantum fluctuations are scaled with temperature in thermal states. It provides a new framework to investigate the thermodynamic properties of quantum systems using quantum metrology.

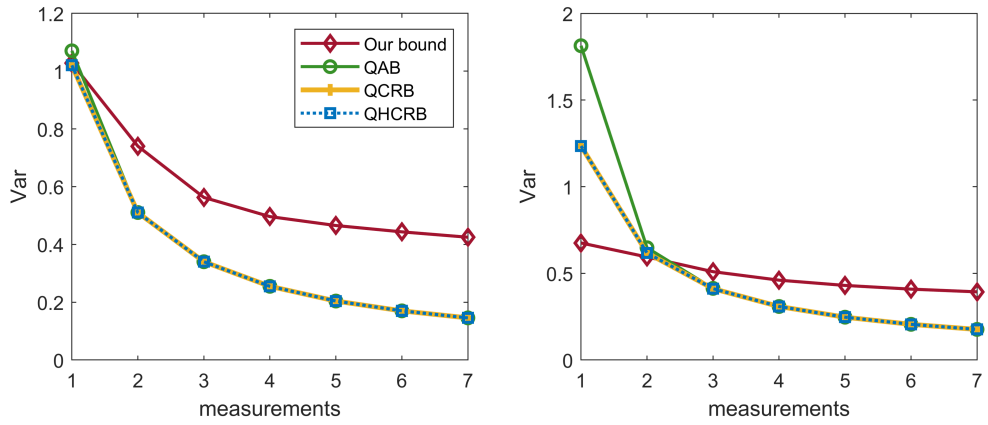

Figure 2: The variance of m-shot scenarios by using m independent copies of the same qubit and joint measurements. The initial Bloch vector is chosen as $r_0 = 0.99$. The rotation axis is $\mathbf{n} = (0, 0, 1)$. In the m-shot case, the phase is set as $-\frac{\pi}{3}$.

5 Application: quantum phase estimation

In this section, we consider a specific application of the proposed theory to quantum parameter estimation. The goal is to estimate an unknown phase parameter θ encoded in a qubit state.

Set the initial single-qubit state as $\rho_0 = \frac{1}{2}(\mathbb{1} + \mathbf{r_0} \cdot \boldsymbol{\sigma})$, where $\mathbf{r_0} = (r_x, r_y, r_z)$ is the Bloch vector with $r_{x(y,z)} = \mathrm{Tr}(\rho_0 \sigma_{x(y,z)})$, and $\boldsymbol{\sigma} = (\sigma_x, \sigma_y, \sigma_z)$ denotes the Pauli vector. The qubit undergoes a unitary rotation $U(\theta) = e^{-i\mathbf{n}\cdot\boldsymbol{\sigma}\theta/2}$, where the unit vector $\mathbf{n}$ defines the rotation axis. The final state after rotation is $\rho_\theta = U(\theta)\rho_0 U^\dagger(\theta) = \frac{1}{2}(\mathbb{1} + \mathbf{r}_\theta \cdot \boldsymbol{\sigma})$.

In the following experiments, the initial Bloch vector is chosen as $\mathbf{r} = (0, r_0, 0)$ and the rotation axis is the Pauli z-axis, i.e., $\mathbf{n} = (0, 0, 1)$. We first provide a theoretical analysis in the case of multiple copies. Then, considering the limitations of our platform in performing joint multi-qubit measurements, we conduct an experimental validation based on repeated single-qubit measurements. We compare the proposed theoretical result with established hierarchical frequentist bounds, including (1) QCRB [37, 38], (2) the lowest order of quantum Barankin bounds (that is, the quantum Hammersley-Chapman-Robbins bound, here we denote as QHCRB). [22, 24, 27], and (3) the lowest order of quantum Abel bounds (here we denote as QAB). [22, 25].

5.1 Theoretical analysis for the multi-copy case

To analyze the asymptotic behavior, we analytically compare the bounds for m independent copies of the same qubit, denoted as $\rho^{\otimes m}$. The present high-order information is not additive, but repeating joint measurements can reduce the average estimation error, as illustrated in Figure 2. Here, we optimize the bounds over general joint measurement operators. The measurement operator M is chosen as $M = |s\rangle\langle s|$, where $|s\rangle = \frac{1}{\sqrt{m}} \sum_{i=1}^{m} |\psi_i\rangle$, and $|\psi_i\rangle$ denotes the i-th qubit is in the state $|1\rangle$ and all the other qubits are in the state $|0\rangle$. This demonstrates that the present bound is tighter than other bounds before reaching the asymptotic limit, where the maximum-likelihood estimator asymptotically converges.

5.2 Experimental validation for the Single-qubit case

5.2.1 Experimental setup

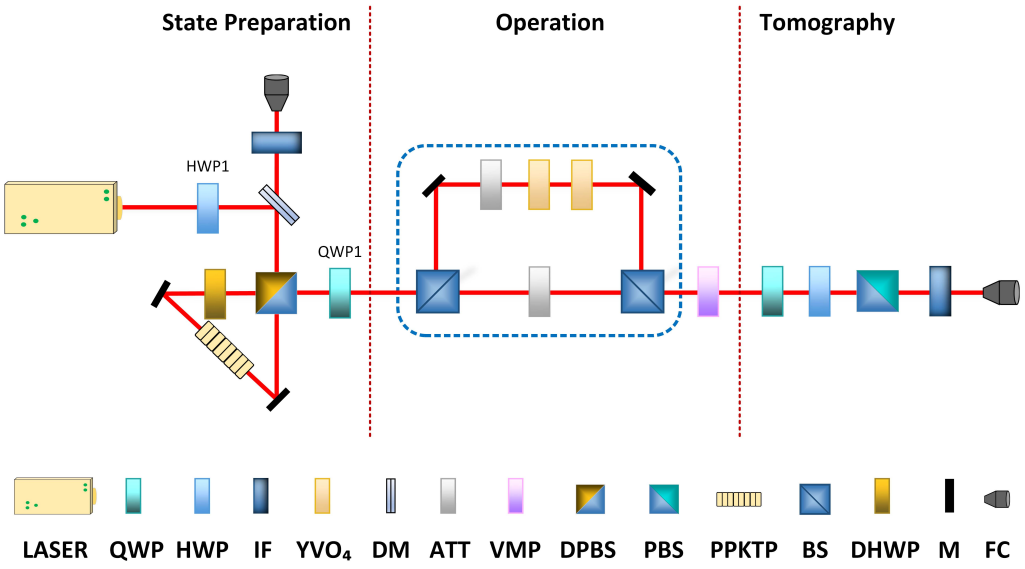

Figure 3: Experimental setup, which includes three modules: (a) state preparation module, (b) white-noise insertion and phase-shift control module, (c) quantum state tomography module. In module (a), a pair of maximally polarization-entangled states is generated by a spontaneous parametric down-conversion process at the dual-wavelength polarization beam splitter (DPBS). A quarter-wave plate (QWP1) is then used to prepare the initial single-photon state $|R\rangle = \frac{1}{\sqrt{2}}(|H\rangle + i|V\rangle)$. To produce the single-photon mixed state, the attenuators (ATTs) are used to regulate the mixed weight p of the states. The density matrix is constructed via the quantum state tomography module (c). Key optical elements include half-wave plate (HWP), interference filter (IF), yttrium orthovanadate (YVO_4), dichromatic mirror (DM), full-wave liquid-crystal variable wave plate (VWP), polarizing beam splitter (PBS), beam splitter (BS), mirror (M), dual-wavelength half-wave plate (DHWP), and fiber coupler (FC).

The experiment was conducted using the photonic platform shown in Figure 3. The experimental setup consists of three primary components: (1) photon source, (2) white-noise insertion and phase-shift control, and (3) quantum tomography. First, the state-preparation module generates an initial pure state $|\Phi\rangle$. In the white-noise module (dashed blue box), the reflected path dephases one photon into a fully mixed state $\frac{1}{2}\mathbb{I}$. The attenuators (ATTs) are employed to adjust the weight p of the mixed state. The controllable rotation $U(\theta)$ is then introduced using a full-wave liquid-crystal variable wave plate (VWP). In the last part, photon-product measurements are performed by setting the angles of the optical axes of the half-wave plate (HWP) and the quarter-wave plate (QWP).

In the state preparation module shown in Figure 3, a type-II phase-matched periodically poled $KTiOPO_4$ (PPKTP) crystal with dimensions $15 \times 2 \times 1$ mm^3 is pumped with a 36 mW diode laser beam to generate photon pairs with a central wavelength of 810 nm via the process of spontaneous parametric down-conversion (SPDC). HWP1 in front of the PPKTP crystal is used to control the generated photon pairs, which are encoded in the polarization degree of freedom as $\frac{1}{\sqrt{2}}(|HV\rangle + |VH\rangle)$. One photon acts as a trig-

ger, and the other serves as a signal photon which is further transformed into the state $|R\rangle = \frac{1}{\sqrt{2}}(|H\rangle + i|V\rangle)$ by QWP1.

To generate a set of noisy states

$$\rho(p) = p|R\rangle\langle R| + \frac{1-p}{2}\mathbb{I} \tag{11}$$

where $\mathbb{I}$ denotes the identity operator of rank 2. As shown in Fig.3, two 50/50 beam splitters (BS) are inserted into the signal branch of the optical setup. In the transmitted path, the photon is prepared in the state $|R\rangle$. In the reflected path, two 2.6 mm yttrium orthovanadate (YVO_4) crystals dephase the single-photon state into the maximally mixed state $\frac{\mathbb{I}}{2}$. The ratio of these two components is controlled by two attenuators (ATTs) at the output port of the second BS. After the insertion of white noise, a controllable phase shift θ is introduced using a full-wave liquid crystal variable wave plate (VWP), which results in the final state $\rho(p,\theta) = U(\theta)\rho(p)U^\dagger(\theta)$.

where the rotation is parameterized with a unitary matrix $U(\theta) = e^{-i\mathbf{n}\cdot\boldsymbol{\sigma}\theta/2}$. The VWP enables rapid phase adjustments, with θ switching within approximately 2 ms, allowing for real-time adaptive feedback. This photon source achieves high brightness (0.34 MHz) and a collection efficiency of 60%.

Tomographic measurements are conducted on single signal photons, employing a post-selection strategy based on 100 sets of photon coincidences. The measurement results are recorded in coincidence with the trigger photons. Utilizing a 3 nm interference filter, the photon source generates up to 15,000 coincidence counts per second. The conditional probability $P(a|x)$ of the outcome $a \in \{-1, +1\}$ is calculated as

$$p(a|x) = \frac{N_x^a}{N_x^{-1} + N_x^{+1}} \tag{12}$$

where N_x^a denotes the photon coincidence counts. The density matrix is reconstructed using maximum-likelihood estimation [39].

5.2.2 Experiment results

We first constructed a set of mixed states $\rho(p)$ by setting different mixture probabilities $\{p, 1-p\}$ for photons from two paths in the second module. The prepared state of a single photon can be represented as $\rho_0 = \frac{1}{2}(\mathbb{I} + \mathbf{r}_0 \cdot \boldsymbol{\sigma})$. After the preparation stage, we implemented a phase rotation with $\theta = \pi$ along the Pauli z-axis, and obtained the output state as $\rho_\theta = \frac{1}{2}(\mathbb{I} + \mathbf{r}_\theta \cdot \boldsymbol{\sigma})$ with $\mathbf{r}_\theta = (-r_0 \sin\theta, r_0 \cos\theta, 0)$.

To experimentally estimate the phase, we first performed the Pauli measurements σ_x, σ_y, and σ_z on each prepared photon. We obtained the Pauli vector as $\mathbf{r}_\theta = (\langle\sigma_x\rangle, \langle\sigma_y\rangle, \langle\sigma_z\rangle)$ and further constructed the density matrices of the encoded states. We compared the present bound with well-known quantum bounds, including QCRB [3], quantum Hammersley-Chapman-Robbins bound (QHCRB) [23, 24, 26, 27], and quantum Abel bound (QAB) [22, 25].

To verify the present bound using the high-order information, we evaluated the second-order information of the phase according to Eq.(3) (see computational details in Appendix D). We finally evaluated the variance according to Eq.(5) by computing the bias parameter $\mathbb{E}[I^q]$, which can be achieved by choosing the Pauli measurements. The error bar is evaluated using the experimental data.

All the fidelities of prepared initial states exceed 99% according to the formula [40]:

$$F(\rho_{\text{exp}}, \rho_{\text{ideal}}) = \text{Tr}\left(\sqrt{\sqrt{\rho_{\text{ideal}}}\rho_{\text{exp}}\sqrt{\rho_{\text{ideal}}}}\right)^2 \tag{13}$$

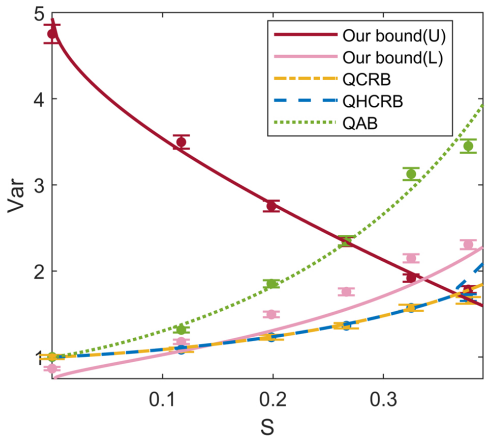

Figure 4: Hierarchic bounds of the variance in terms of the length of Pauli vector $\mathbf{r}_0$ in both the ideal case (lines) and experimental case (dots). We verify the hierarchic quantum bounds including QCRB (yellow dashed line) [3], quantum Hammersley-Chapman-Robbins bound (QHCRB, blue dashed line) [23,24,26,27], and quantum Abel bound (QAB, green dotted line) [22,25], and the present bound (red and pink lines). For the red line, we choose Pauli x measurement and get the value of $\{\mathbb{E}_{I^q}\}$ at each data point. For the pink line, we constrain the value of $\mathbb{E}_{I^q}$ as the average of $\{\mathbb{E}_{I^q}\}$ at all data points. The initial Pauli vector is choose as $\mathbf{r}_0 = (0, r_0, 0)$ and the rotation is $U(\pi)$ along the Pauli z-axis.

(see data in Appendix E). All the estimated bounds of the variances are shown in Figure 4. This implies the following supremacy of the present method. Firstly, the variance from the present method is greatly larger than all the other bounds when the entropy $S(\rho)$ is no more than 2.5. This means that the present method shows great improvement for quantum phase estimation with limited noise. Moreover, while all the previous bounds are evaluated from the standard FI, our method depends on the high-order information of the phase from a new score function. This means that the present score function shows different features of the estimated phase and provides a great advantage beyond linear estimators [3, 22–27]. Beyond, our method provides another level of error bound with respect to all the existing hierarchical quantum bounds, with an error bar no more than 0.2657. In experiments, we choose the single photon to verify the QCRB in a one-shot manner. A further experiment should be interesting by implementing joint measurement on multiple copies of single particles.

6 Conclusion

In contrast to CRB, the present bound is derived using extendable higher-order derivatives of the estimating function, rather than relying directly on the PDF of the estimated parameters. While the CRB is particularly effective for PDFs that approximate a normal distribution, the inclusion of higher-order derivative information in the present method handles complex distributions well. This approach leverages the attainability condition to provide deeper insights into the structure and properties of estimators.

Although the present high-order information is not additive, the simulations demonstrate that the derived estimation bound asymptotically behaves like the FI and converges to the QCRB for independent and identically distributed data. This asymptotic conver-

gence underscores its practical utility and effectiveness in applications, particularly in situations where higher-order information plays a crucial role. Another important challenge is to incorporate biased estimation scenarios, offering insights into how biases affect the proposed second-order metric.

In summary, by extending the foundational concepts of FI to incorporate second-order effects, we have proposed a novel framework that enhances both the theoretical and practical understanding of classical and quantum estimation processes. Specifically, we introduced an operational quantity based on the second-order derivative of the estimator, referred to as the second-order information. This new quantity provides a deeper and more comprehensive analysis of a system's behavior when combined with the FI and its quantum extensions, offering valuable insights into estimation processes and their underlying structures.

Author contributions X.Z. and Y.H. conducted the experiments. M.X.L. conducted the research. All authors wrote and reviewed the manuscript.

Funding information This work was supported by the National Natural Science Foundation of China (Nos.61772437, 12204386, 12075159, and 12171044), Sichuan Natural Science Foundation (No.2023NSFSC0447), Beijing Natural Science Foundation (No.Z190005), Interdisciplinary Research of Southwest Jiaotong University China Interdisciplinary Research of Southwest Jiaotong University China (No.2682022KJ004), and the Academician Innovation Platform of Hainan Province.

A Classical metrology with high order information

In this section, we show classical metrology with high-order information and give the conditions of asymptotic attainability.

A.1 New bound of classical metrology with high order information

Consider a parametric model $\{p_\theta(x) : \theta \in \Omega\}$, where θ is a single parameter and Ω is a subset of $\mathbb{R}$. Define $\hat{\theta}$ as an unbiased estimator of θ, satisfying $\mathbb{E}_X[\hat{\theta}(X)] = \theta$ for $\theta \in \Omega$. Define the second-order information depending on the second derivative of the root score function as

$$I_2 = 4 \int \left(\partial_\theta^2 \sqrt{p_\theta(x)}\right)^2 dx, \tag{A.1}$$

where we have assumed the given statistical function $p_\theta(x)$ has the second-order derivative.

From the assumption of the unbiased estimation, we obtain

$$\mathbb{E}_X[\hat{\theta}(X) - \theta] = \int \left(\hat{\theta}(x) - \theta\right) p_\theta(x) dx = 0. \tag{A.2}$$

By taking the derivative of θ, from Leibniz's Rule, we obtain that

$$\partial_\theta \int (\hat{\theta}(x) - \theta) p_\theta(x) dx = \int (\hat{\theta}(x) - \theta) \partial_\theta p_\theta(x) dx - \int p_\theta(x) dx = 0. \tag{A.3}$$

This implies that

$$\int (\hat{\theta}(x) - \theta) \partial_\theta p_\theta(x) dx = 1. \tag{A.4}$$

Now, we perform the derivative of θ on two sides of Eq.(A.4) and obtain that

$$\int \left(\hat{\theta}(x) - \theta\right) \partial_\theta^2 p_\theta(x) dx - \int \partial_\theta p_\theta(x) dx = 0, \tag{A.5}$$

which is equivalent to the following equality as

$$\int \left(\hat{\theta}(x) - \theta\right) \partial_\theta^2 p_\theta(x) dx = 0. \tag{A.6}$$

where we have used the equalities $\int p_\theta(x)dx = 1$ and $\int \partial_\theta p_\theta(x)dx = 0$.

For any probability function $p_\theta(x)$ with second-order derivative, it follows that

$$\begin{aligned} \partial_\theta^2 p_\theta(x) &= \partial_\theta^2(\sqrt{p_\theta(x)}\sqrt{p_\theta(x)}) \\ &= 2\left(\partial_\theta \sqrt{p_\theta(x)}\right)^2 + 2\sqrt{p_\theta(x)}\partial_\theta^2\sqrt{p_\theta(x)}. \end{aligned} \tag{A.7}$$

Substituting Eq.(A.7) into Eq.(A.6) implies that

$$\int (\hat{\theta}(x) - \theta)\left(\partial_\theta \sqrt{p_\theta(x)}\right)^2 dx + \int (\hat{\theta}(x) - \theta)\sqrt{p_\theta(x)}\partial_\theta^2\sqrt{p_\theta(x)}dx = 0, \tag{A.8}$$

$$\int (\hat{\theta}(x) - \theta)\left(\partial_\theta \sqrt{p_\theta(x)}\right)^2 dx = \int (\theta - \hat{\theta}(x))\sqrt{p_\theta(x)}\partial_\theta^2\sqrt{p_\theta(x)}dx. \tag{A.9}$$

Consider the left side of Eq.(A.9). Define

$$\mathbb{E}_X[I_{\hat{\theta}}(X)] = \int (\hat{\theta}(x) - \theta) I(x, \theta) dx, \tag{A.10}$$

where $I(x, \theta) = (\partial_\theta \sqrt{p_\theta(x)})^2$, which can be regarded as the density of FI. Applying the Cauchy-Schwarz inequality: $\int fgdx \leq \sqrt{\int f^2 dx \int g^2 dx}$ to the second item of the left side of Eq.(A.9), we obtain that

$$\begin{aligned} \left|\int (\theta - \hat{\theta}(x))\sqrt{p_\theta(x)}\partial_\theta^2\sqrt{p_\theta(x)}dx\right| &\leq \sqrt{\int (\hat{\theta}(x) - \theta)^2 p_\theta(x)dx}\sqrt{\int \left(\partial_\theta^2\sqrt{p_\theta(x)}\right)^2 dx} \\ &= \frac{1}{2}\sqrt{\Delta\hat{\theta}^2}\sqrt{I_2}, \end{aligned} \tag{A.11}$$

where $\Delta\hat{\theta}^2 = \int (\hat{\theta}(x) - \theta)^2 p_\theta(x)dx$ denotes the variance of the estimation $\hat{\theta}$ and I_2 is the second-order information defined in Eq.(A.1). Combining both Eqs.(A.10,A.11) implies that

$$\Delta\hat{\theta} \geq \frac{2|\mathbb{E}_X[I_{\hat{\theta}}(X)]|}{\sqrt{I_2}}. \tag{A.12}$$

This implies that

$$\Delta\hat{\theta}^2 \geq \frac{4\mathbb{E}_X[I_{\hat{\theta}}(X)]^2}{I_2}. \tag{A.13}$$

Now, when it comes to a point estimation, we prove the more precise bound for $\mathbb{E}_X[I_{\hat{\theta}}(X)]^2$. In fact, by using the Cauchy-Schwarz inequality to the first item of the

left side of Eq.(A.9), it follows that

$$\begin{aligned}\int (\hat{\theta}(x)-\theta)\left(\partial_\theta\sqrt{p_\theta(x)}\right)^2 dx &= \int \hat{\theta}(x)\left(\partial_\theta\sqrt{p_\theta(x)}\right)^2 dx - \theta\int\left(\partial_\theta\sqrt{p_\theta(x)}\right)^2 dx \\ &\leq \sqrt{\int \hat{\theta}(x)^2 dx \int\left(\partial_\theta\sqrt{p_\theta(x)}\right)^4 dx} - \frac{\theta}{4}\mathbb{I} \\ &= c_I\sqrt{\int \hat{\theta}(x)^2 dx\left(\int\left(\partial_\theta\sqrt{p_\theta(x)}\right)^2 dx\right)^2} - \frac{\theta}{4}\mathbb{I} \\ &= c_I\frac{1}{4}\sqrt{\int \hat{\theta}(x)^2 dx I^2} - \frac{\theta}{4}\mathbb{I} \\ &= c_I\frac{I}{4}\left(\sqrt{\int \hat{\theta}(x)^2 dx} - \theta\right), \end{aligned} \tag{A.14}$$

where c_I is a constant determined by the integral interval. Adding up Eqs.(A.11,A.14) implies that

$$0 \leq \sqrt{\Delta\hat{\theta}^2}\sqrt{I_2} + c_I\frac{\|\hat{\theta}\|_2 - \theta}{2}I, \tag{A.15}$$

where $\|\hat{\theta}\|_2^2 = \int \hat{\theta}(x)^2 dx$.

Similarly, it follows that

$$0 \leq \sqrt{\Delta\hat{\theta}^2}\sqrt{I_2} + c_I\frac{\theta - \|\hat{\theta}\|_2}{2}I. \tag{A.16}$$

Combining both the inequalities (A.15) and (A.16) yields

$$\Delta\hat{\theta}^2 \geq c_I(\theta - \|\hat{\theta}\|_2)^2\frac{I^2}{4I_2}. \tag{A.17}$$

This has completed the proof.

A.2 The attainability conditions

In this subsection, we show the conditions of attainability. Specifically, the saturable condition of the inequality (A.11) is:

$$\partial_\theta^2\sqrt{p_\theta(x)} = \frac{1}{C}(\theta - \hat{\theta}(x))\sqrt{p_\theta(x)}, \tag{A.18}$$

where C is a constant.

Let $\sqrt{p_\theta(x)} = q_\theta(x)$. It follows that

$$\partial_\theta^2 q_\theta(x) - \frac{(\theta - \hat{\theta}(x))}{C}q_\theta(x) = 0. \tag{A.19}$$

Assume a solution is given by $q_\theta(x) = e^{r\theta}$. Substituting into the differential equation (A.19) gives:

$$r^2 e^{r\theta} - \frac{(\theta - \hat{\theta}(x))}{C}e^{r\theta} = 0. \tag{A.20}$$

This implies the characteristic equation as $r = \pm\sqrt{\frac{\theta-\hat{\theta}(x)}{C}}$. This further gives a general solution to the homogeneous equation as

$$q_\theta(x) = C_1 e^{\sqrt{\frac{\theta-\hat{\theta}(x)}{C}}\theta} + C_2 e^{-\sqrt{\frac{\theta-\hat{\theta}(x)}{C}}\theta}, \tag{A.21}$$

where C_1 and C_2 are arbitrary non-zero constants. So, the final condition is given by

$$p_\theta(x) = \left((C_1 + C_2 e^{-\theta})e^{-\sqrt{\frac{\theta-\hat{\theta}(x)}{C}}}\right)^2. \tag{A.22}$$

This saturable condition for classical metrology with high-order information implies that $p_\theta(x)$ is a non-Gaussian distribution.

B Proof of the main result

Now, we prove the inequality (5).

First, note that

$$\partial_\theta \rho_\theta = \partial_\theta\sqrt{\rho_\theta}\sqrt{\rho_\theta} + \sqrt{\rho_\theta}\partial_\theta\sqrt{\rho_\theta} \tag{B.1}$$

By taking the second derivative of parameter θ in Eq.(B.1), we obtain that

$$\partial_\theta^2\rho_\theta = (\partial_\theta^2\sqrt{\rho_\theta})\sqrt{\rho_\theta} + 2(\partial_\theta\sqrt{\rho_\theta})^2 + \sqrt{\rho_\theta}\partial_\theta^2\sqrt{\rho_\theta} \tag{B.2}$$

Given an unbiased measurement M, i.e., $\mathrm{Tr}(M\rho_\theta) = \theta$ for $\theta \in \Omega$, it shows that $\mathrm{Tr}(M\partial_\theta^2\rho_\theta) = 0$. For any quantum state ρ_θ we have $\mathrm{Tr}\rho_\theta = 1$ and $\mathrm{Tr}\partial_\theta^2\rho_\theta = 0$. This implies that

$$\mathrm{Tr}(\hat{M}\partial_\theta^2\rho_\theta) = 0 \tag{B.3}$$

with $\hat{M} = M - \theta$.

According to the triangle inequality $|x+y| \leq |x| + |y|$ we obtain from Eq.(B.2) that

$$|\mathrm{Tr}(\hat{M}(\partial_\theta^2\sqrt{\rho_\theta})\sqrt{\rho_\theta})| + |\mathrm{Tr}(\hat{M}\sqrt{\rho_\theta}\partial_\theta^2\sqrt{\rho_\theta})| + 2|\mathrm{Tr}(\hat{M}(\partial_\theta\sqrt{\rho_\theta})^2)| \geq 0 \tag{B.4}$$

Using the Cauchy-Schwarz inequality of $|\mathrm{Tr}(AB)| \leq \sqrt{\mathrm{Tr}(AA^\dagger)\mathrm{Tr}(BB^\dagger)}$ for two matrices A and B in the first term in the left side of Eq.(B.4), we obtain that

$$\begin{aligned}\left|\mathrm{Tr}(\hat{M}(\partial_\theta^2\sqrt{\rho_\theta})\sqrt{\rho_\theta})\right|^2 &\leq \mathrm{Tr}(\sqrt{\rho_\theta}\hat{M}\hat{M}^\dagger(\sqrt{\rho_\theta})^\dagger)\mathrm{Tr}(\partial_\theta^2\sqrt{\rho_\theta})^2 \\ &= \mathrm{Tr}(\rho_\theta\hat{M}^2)\mathrm{Tr}(\partial_\theta^2\sqrt{\rho_\theta}))^2\end{aligned} \tag{B.5}$$

Also, we have

$$\mathrm{Tr}(\rho_\theta\hat{M}^2) = \mathrm{Tr}(\rho_\theta M^2) - (\mathrm{Tr}\rho_\theta M)^2 = \Delta M^2 \tag{B.6}$$

Combining Eqs.(B.5) and (B.6), we obtain that

$$\left|\mathrm{Tr}(\hat{M}\partial_\theta^2\sqrt{\rho_\theta}\sqrt{\rho_\theta})\right|^2 \leq \frac{1}{4}\Delta M^2 I_2^q \tag{B.7}$$

The second item on the left side of Eq.(B.4) can be calculated in the same way as

$$\left|\mathrm{Tr}(\hat{M}\sqrt{\rho_\theta}\partial_\theta^2\sqrt{\rho_\theta})\right|^2 \leq \mathrm{Tr}(\hat{M}^2\rho_\theta)\mathrm{Tr}(\partial_\theta^2\sqrt{\rho_\theta})^2 \tag{B.8}$$

Combining Eqs.(B.4,B.7,B.8) implies the first result as

$$\Delta M^2 \geq \frac{4\mathbb{E}[I^q]^2}{I_2^q} \tag{B.9}$$

For the special case of estimating a parameter at a fixed point, the last item in Eq.(B.4) can be rewritten into

$$\begin{aligned} \mathrm{Tr}(\hat{M}(\partial_\theta\sqrt{\rho_\theta})^2) &\leq \sqrt{\mathrm{Tr}M^2}\sqrt{\mathrm{Tr}(\partial_\theta\sqrt{\rho_\theta})^4} - \frac{\theta}{4}I^q \\ &\leq \|M\|_F\sqrt{(\mathrm{Tr}(\partial_\theta\sqrt{\rho_\theta})^2)^2} - \frac{\theta}{4}I^q \\ &= \frac{\|M\|_F - \theta}{4}I^q \end{aligned} \tag{B.10}$$

where the inequalities are based on the matrix inequality of $(\mathrm{Tr}A^2)^2 \geq \mathrm{Tr}A^4$ for any matrix A.

Finally, from Eqs. (B.4,B.10), we obtain the second result as

$$\Delta M^2 \geq (\theta - \|M\|_F)^2\frac{(I^q)^2}{4I_2^q} \tag{B.11}$$

Compared with the quantum Cramér-Rao bound (QCRB) for characterizing an unbiased estimator [3,4], the inequality (5) provides an approach to feature estimation accuracy by incorporating both the first-order and second-order information. This framework enables a more refined analysis of parameter estimation, and can achieve better precision than the well-known results in quantum metrology [3, 4, 41, 42], see the following example of quantum phase estimation.

C Evaluation of high-order quantum information

The standard definition of QFI is given by $F_q = \langle L^2\rangle = 2\mathrm{Tr}(\rho L^2)$ [43], where L is so-called symmetric logarithmic derivative (SLD). Denoting the parameter under the estimation as θ, the SLD operator is determined by the equation $\partial_\theta\rho = \frac{1}{2}(\rho L + L\rho)$. We extend the SLD by using the following equation:

$$\partial_\theta\sqrt{\rho} = \frac{1}{2}(\sqrt{\rho}L + L\sqrt{\rho}). \tag{C.1}$$

Here, we cannot get the equality of $\langle L\rangle = 0$. We employ the Lyapunov representation [44] to compute the generalized SLD operator. The definition in equation (C.1) is a special form of the Lyapunov equation. To resolve this equation, we define a function as

$$f(s) = e^{-\sqrt{\rho}s}Le^{-\sqrt{\rho}s}, \tag{C.2}$$

where f satisfies $f(0) = L$. The partial derivative of $f(s)$ on s is given by

$$\partial_s f(s) = -2e^{-\sqrt{\rho}s}(\partial_\theta\sqrt{\rho})e^{-\sqrt{\rho}s}. \tag{C.3}$$

Integrating both sides of this equation implies that

$$f(\infty) - f(0) = -2\int_0^\infty e^{-\sqrt{\rho}s}(\partial_\theta\sqrt{\rho})e^{-\sqrt{\rho}s}ds. \tag{C.4}$$

When ρ is full rank, $e^{-\sqrt{\rho}s}$ trends to zero for $s \to \infty$, which implies that $f(\infty) = 0$. This yields to the generalized SLD operator as

$$L = 2\int_0^\infty e^{-\sqrt{\rho}s}(\partial_\theta\sqrt{\rho})e^{-\sqrt{\rho}s}ds, \tag{C.5}$$

which provides a basis-independent representation. When ρ is non-full rank, the generalized SLD operator can be decomposed into four blocks [45], which can follow the same form as Eq.(C.5).

Moreover, from Eq.(C.1) we obtain that

$$\begin{aligned}\partial_\theta^2\sqrt{\rho} &= \frac{1}{2}(\partial_\theta\sqrt{\rho}L + \sqrt{\rho}\partial_\theta L + \partial_\theta L\sqrt{\rho} + L\partial_\theta\sqrt{\rho}) \\ &= \frac{1}{2}\{\partial_\theta L, \sqrt{\rho}\} + \frac{1}{2}\{\{L, \sqrt{\rho}\}, L\},\end{aligned} \tag{C.6}$$

where $\{\cdot,\cdot\}$ denotes the anti-commutator. By using the spectral decomposition form $\rho = \sum_i \lambda_i|\varphi_i\rangle\langle\varphi_i|$, the element of generalized SLD operator can be expressed by

$$L_{ij} = \frac{\partial_\theta\lambda_i}{\lambda_i}\delta_{ij} + \frac{2(\lambda_i - \lambda_j)}{\lambda_i + \lambda_j}\langle\partial_\theta\varphi_i|\varphi_j\rangle, \tag{C.7}$$

where λ_i, $|\varphi_i\rangle$ are the i-th eigenvalue and eigenstate of ρ, respectively. Combining with Eq.(C.6), one can get the element of $\partial_\theta^2\sqrt{\rho}$, which further implies the evaluation of the second-order quantum information as

$$\begin{aligned}I_2^q &= \sum_{i,j}(p_i''p_j''a_{ij} + 2p_i''p_j'a'_{j|i} + p_i''p_ja''_{j|i} + 2p_i'p_j''a'_{i|j} + 4p_i'p_j'a'_{ij} \\ &\quad +2p_i'p_jb_{i|j} + p_ip_j''a''_{i|j} + 2p_ip_j'b_{j|i} + p_ip_jb_{ij}),\end{aligned} \tag{C.8}$$

where $p_i = \sqrt{\lambda_i}$, $p_i' = \partial_\theta p_i$, $p_i'' = \partial_\theta^2 p_i$, $a_{ij} = \mathrm{Tr}|\varphi_i\rangle\langle\varphi_i|\varphi_j\rangle\langle\varphi_j|$, $a'_{ij} = \mathrm{Tr}(|\varphi_i\rangle\langle\varphi_i|)'(|\varphi_j\rangle\langle\varphi_j|)'$, $b_{ij} = \mathrm{Tr}(|\varphi_i\rangle\langle\varphi_i|)''(|\varphi_j\rangle\langle\varphi_j|)''$, $a'_{i|j} = \mathrm{Tr}(|\varphi_i\rangle\langle\varphi_i|)'|\varphi_j\rangle\langle\varphi_j|$, $a''_{i|j} = \mathrm{Tr}(|\varphi_i\rangle\langle\varphi_i|)''|\varphi_j\rangle\langle\varphi_j|$, and $b_{i|j} = \mathrm{Tr}(|\varphi_i\rangle\langle\varphi_i|)'(|\varphi_j\rangle\langle\varphi_j|)''$.

D Estimating the phase of single qubit

Consider an application of the quantum phase estimation. Given a single qubit along the Pauli-y axis, its state can be represented by $\rho = \frac{1}{2}(\mathbb{1} + \mathbf{r}_0 \cdot \vec{\sigma})$, where $\vec{\sigma} = (\sigma_x, \sigma_y, \sigma_z)$ is a vector of Pauli matrices, and $\mathbf{r}_0 = (0, r_0, 0)^\top$ with $r_0 \in [0, 1]$. Suppose it undergoes a rotation along the Pauli-z axis, denoted as $U(\theta) = e^{-i\sigma_z\theta/2}$. The final state is given by $\rho(\theta) = U(\theta)\rho U^\dagger(\theta) := \frac{1}{2}(\mathbb{1} + \mathbf{r}_\theta \cdot \vec{\sigma})$, where the rotated Bloch vector is given by $\mathbf{r}_\theta = \cos\theta(\mathbf{r}_0 - (\mathbf{n}\cdot\mathbf{r}_0)\mathbf{n}) + (\mathbf{n}\cdot\mathbf{r}_0)\mathbf{n} + \sin\theta(\mathbf{n}\times\mathbf{r}_0)$. The goal is to estimate the phase parameter θ.

We compare our bound correlated to high-order information with hierarchies of typical frequentist bounds [22].

According to the result in the main text, we obtain that

$$\Delta M^2 \geq \frac{4\mathbb{E}[I^q]^2}{I_2^q}, \tag{D.1}$$

where $\mathbb{E}[I^q] = \mathrm{Tr}((M-\theta)(\partial_\theta\sqrt{\rho_\theta})^2)$. As for the qubit state, we obtain that

$$\partial_\theta\mathbf{r}_\theta = -\sin\theta(\mathbf{r}_0 - (\mathbf{n}\cdot\mathbf{r}_0)\mathbf{n}) + \cos\theta(\mathbf{n}\times\mathbf{r}_0), \tag{D.2}$$

$$\partial_\theta^2\mathbf{r}_\theta = -\cos\theta(\mathbf{r}_0 - (\mathbf{n}\cdot\mathbf{r}_0)\mathbf{n}) - \sin\theta(\mathbf{n}\times\mathbf{r}_0). \tag{D.3}$$

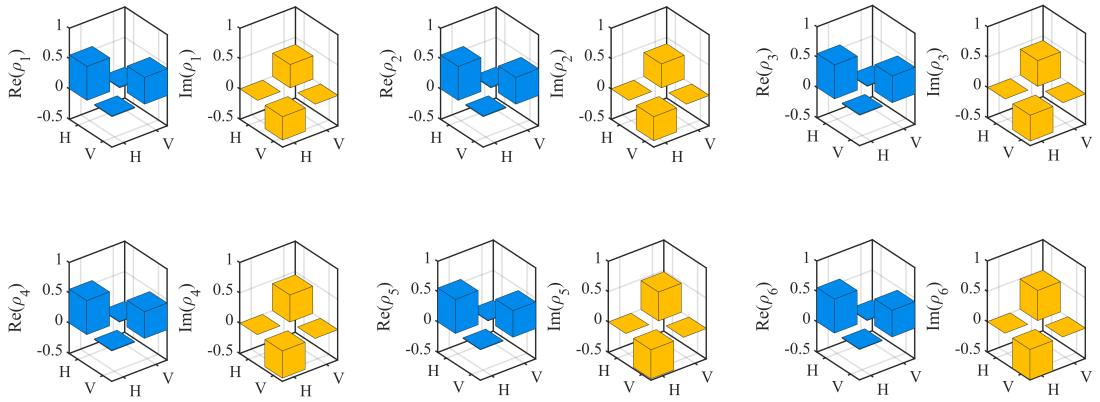

Figure 5: The tomographic results for all the experimental photon states.

Table 1: Fidelity of experimental single qubit states.

r_0	0.7500	0.8000	0.8500
Fidelity	0.9953 ± 0.0024	0.9956 ± 0.0038	0.9954 ± 0.0030
r_0	0.9000	0.9500	1.0000
Fidelity	0.9953 ± 0.0049	0.9949 ± 0.0032	0.9955 ± 0.0036

Note the single qubit can be decomposed by $\rho_\theta = \sum_\pm \lambda_\pm |\psi_\pm\rangle\langle\psi_\pm|$, where $\lambda_\pm = \frac{1\pm|\mathbf{r}_\theta|}{2}$ and $|\psi_\pm\rangle\langle\psi_\pm| = \frac{1}{2}(\mathbb{1} \pm \frac{\mathbf{r}_\theta\cdot\vec{\sigma}}{|\mathbf{r}_\theta|})$. This further implies that

$$\begin{aligned}
\sqrt{\rho_\theta} &= \frac{1}{2}\left(\left(\sqrt{\frac{1+|\mathbf{r}_\theta|}{2}}+\sqrt{\frac{1-|\mathbf{r}_\theta|}{2}}\right)\mathbb{1}+\left(\sqrt{\frac{1+|\mathbf{r}_\theta|}{2}}-\sqrt{\frac{1-|\mathbf{r}_\theta|}{2}}\right)\cdot\frac{\mathbf{r}_\theta}{|\mathbf{r}_\theta|}\cdot\vec{\sigma}\right),\\
\partial_\theta\sqrt{\rho_\theta} &= \frac{1}{2}\left(\sqrt{\frac{1+|\mathbf{r}_\theta|}{2}}-\sqrt{\frac{1-|\mathbf{r}_\theta|}{2}}\right)\frac{1}{|\mathbf{r}_\theta|}\cdot\partial_\theta\mathbf{r}_\theta\cdot\vec{\sigma},\\
\partial_\theta^2\sqrt{\rho_\theta} &= \frac{1}{2}\left(\sqrt{\frac{1+|\mathbf{r}_\theta|}{2}}-\sqrt{\frac{1-|\mathbf{r}_\theta|}{2}}\right)(-\sin\theta\sigma_x-\cos\theta\sigma_y)
\end{aligned} \tag{D.4}$$

according to the equality of the high-order information $I_2^q = (\sqrt{1+|\mathbf{r}_\theta|}-\sqrt{1-|\mathbf{r}_\theta|})^2$.

E Experimental data

In this section, we supplement some experimental data used in the main text. This includes quantum state tomography, as shown in Fig.5 and fidelities of each quantum state for computing the hierarchical frequentist bounds, as shown in Table 1.

References

[1] H. Cramér, *Mathematical methods of statistics*, vol. 26, Princeton university press (1999).

[2] C. R. Rao, *Information and the accuracy attainable in the estimation of statistical parameters*, In *Breakthroughs in Statistics: Foundations and basic theory*, pp. 235–247. Springer (1992).

[3] C. Helstrom, *Quantum detection and estimation theory*, J. Stat. Phys. **1**, 231 (1969).

[4] S. L. Braunstein and C. M. Caves, *Statistical distance and the geometry of quantum states*, Phys. Rev. Lett. **72**, 3439 (1994), doi:10.1103/PhysRevLett.72.3439.

[5] L.-Z. Liu, Y.-Z. Zhang, Z.-D. Li, R. Zhang, X.-F. Yin, Y.-Y. Fei, L. Li, N.-L. Liu, F. Xu, Y.-A. Chen *et al.*, *Distributed quantum phase estimation with entangled photons*, Nature photonics **15**(2), 137 (2021), doi:https://doi.org/10.1038/s41566-020-00718-2.

[6] M. Valeri, E. Polino, D. Poderini, I. Gianani, G. Corrielli, A. Crespi, R. Osellame, N. Spagnolo and F. Sciarrino, *Experimental adaptive bayesian estimation of multiple phases with limited data*, npj Quantum Information **6**(1), 92 (2020), doi:https://doi.org/10.1038/s41534-020-00326-6.

[7] P. Yin, X. Zhao, Y. Yang, Y. Guo, W.-H. Zhang, G.-C. Li, Y.-J. Han, B.-H. Liu, J.-S. Xu, G. Chiribella *et al.*, *Experimental super-heisenberg quantum metrology with indefinite gate order*, Nat. Phys. **19**(8), 1122 (2023), doi:https://doi.org/10.1038/s41567-023-02046-y.

[8] V. Giovannetti, S. Lloyd and L. Maccone, *Quantum metrology*, Phys. Rev. Lett. **96**(1), 010401 (2006).

[9] L. A. Correa, M. Mehboudi, G. Adesso and A. Sanpera, *Individual quantum probes for optimal thermometry*, Phys. Rev. Lett. **114**, 220405 (2015).

[10] A. D. Pasquale, D. Rossini, R. Fazio and V. Giovannetti, *Local quantum thermal susceptibility*, Nat. Commun. **7**, 12782 (2016).

[11] I. Lovchinsky, A. O. Sushkov, E. Urbach, N. P. de Leon, S. Choi, K. D. Greve, R. Evans, R. Gertner, E. Bersin, C. Müller, L. McGuinness, F. Jelezko *et al.*, *Nuclear magnetic resonance detection and spectroscopy of single proteins using quantum logic*, Science **351**, 836 (2016).

[12] B. Abbott *et al.*, *Observation of gravitational waves from a binary black hole merger*, Phys. Rev. Lett. **116**, 061102 (2016).

[13] C. L. Degen, F. Reinhard and P. Cappellaro, *Quantum sensing*, Rev. Mod. Phys. **89**, 035002 (2017).

[14] A. Abbas, D. Sutter, C. Zoufal, A. Lucchi, A. Figalli and S. Woerner, *The power of quantum neural networks*, Nature Computational Science **1**(6), 403 (2021).

[15] T. J. Proctor, P. A. Knott and J. A. Dunningham, *Multiparameter estimation in networked quantum sensors*, Phys. Rev. Lett. **120**(8), 080501 (2018).

[16] L. Pezzè, A. Smerzi, M. K. Oberthaler, R. Schmied and P. Treutlein, *Quantum metrology with nonclassical states of atomic ensembles*, Rev. Mod. Phys. **90**, 035005 (2018), doi:10.1103/RevModPhys.90.035005.

[17] F. Casola, T. van der Sar and A. Yacoby, *Probing condensed matter physics with magnetometry based on nitrogen-vacancy centres in diamond*, Nat. Rev. Mater. **3**, 17088 (2018).

[18] C. Couteau, S. Barz, T. Durt, T. Gerrits, J. Huwer, R. Prevedel, J. Rarity, A. Shields and G. Weihs, *Applications of single photons in quantum metrology, biology and the foundations of quantum physics*, Nat. Rev. Phys. **5**(6), 354 (2023), doi:https://doi.org/10.1038/s42254-023-00589-w.

[19] L. McCuller, C. Whittle, D. Ganapathy, K. Komori, M. Tse, A. Fernandez-Galiana, L. Barsotti, P. Fritschel, M. MacInnis, F. Matichard, K. Mason, N. Mavalvala *et al.*, *Frequency-dependent squeezing for advanced ligo*, Phys. Rev. Lett. **124**, 171102 (2020).

[20] E. Polino, M. Valeri, N. Spagnolo and F. Sciarrino, *Photonic quantum metrology*, AVS Quantum Science **2**(2), 024703 (2020), doi:https://doi.org/10.1116/5.0007577.

[21] I. Marvian, *Operational interpretation of quantum fisher information in quantum thermodynamics*, Phys. Rev. Lett. **129**(19), 190502 (2022), doi:https://doi.org/10.1103/PhysRevLett.129.190502.

[22] M. Gessner and A. Smerzi, *Hierarchies of frequentist bounds for quantum metrology: from cramér-rao to barankin*, Phys. Rev. Lett. **130**(26), 260801 (2023).

[23] J. M. Hammersley, *On estimating restricted parameters*, J. Roy. Statist. Soc. Ser. B **12**, 192 (1950).

[24] D. G. Chapman and H. Robbins, *Minimum variance estimation without regularity assumptions*, Ann. Math. Statist. **22**, 581 (1951), doi:10.1214/aoms/1177729548.

[25] J. S. Abel, *A bound on mean square estimate error*, IEEE Trans. Inf. Theory **39**, 1675 (1993), doi:10.1109/18.259655.

[26] A. Bhattacharyya, *On some analogues of the amount of information and their use in statistical estimation*, Sankhyā **8**, 1 (1946).

[27] E. W. Barankin, *Locally best unbiased estimates*, Ann. Math. Stat. **20**, 477 (1949), doi:10.1214/aoms/1177729943.

[28] P. Stoica and B. C. Ng, *On the cramér-rao bound under parametric constraints*, IEEE Signal Proc. Lett. **5**(7), 177 (1998).

[29] Z. Ben-Haim and Y. C. Eldar, *The cramér-rao bound for estimating a sparse parameter vector*, IEEE Trans. Signal Proc. **58**(6), 3384 (2010).

[30] A. Cianchi, E. Lutwak, D. Yang and G. Zhang, *A unified approach to cramér–rao inequalities*, IEEE Trans. Inf. Theory **60**(1), 643 (2013).

[31] R. A. Fisher, *Theory of statistical estimation*, Mathematical Proceedings of the Cambridge Philosophical Society **22**, 700 (1925).

[32] Y. Chu and J. Cai, *Thermodynamic principle for quantum metrology*, Phys. Rev. Lett. **128**(20), 200501 (2022), doi:https://doi.org/10.1103/PhysRevLett.128.200501.

[33] H. J. Miller and J. Anders, *Energy-temperature uncertainty relation in quantum thermodynamics*, Nat. Commun. **9**(1), 2203 (2018), doi:https://doi.org/10.1038/s41467-018-04536-7.

[34] L. Masanes and J. Oppenheim, *A general derivation and quantification of the third law of thermodynamics*, Nat. Commun. **8**(1), 1 (2017).

[35] J. Liu, H. Yuan, X.-M. Lu and X. Wang, *Quantum fisher information matrix and multiparameter estimation*, J. Phys. A: Math. Theore. **53**(2), 023001 (2020).

[36] D. Braun, G. Adesso, F. Benatti, R. Floreanini, U. Marzolino, M. W. Mitchell and S. Pirandola, *Quantum-enhanced measurements without entanglement*, Rev. Mod. Phys. **90**(3), 035006 (2018).

[37] C. M. Helstrom, *Quantum Detection and Estimation Theory*, Academic Press (1976).

[38] S. L. Braunstein and C. M. Caves, *Statistical distance and the geometry of quantum states*, Phys. Rev. Lett. **72**, 3439 (1994), doi:10.1103/PhysRevLett.72.3439.

[39] J. B. Altepeter, E. R. Jeffrey and P. G. Kwiat, *Photonic state tomography*, Advances in Atomic, Molecular, and Optical Physics **52**, 105 (2005), doi:https://doi.org/10.1016/S1049-250X(05)52003-2.

[40] R. Horodecki, P. Horodecki, M. Horodecki and K. Horodecki, *Quantum entanglement*, Rev. Mod. Phys. **81**, 865 (2009), doi:https://doi.org/10.1103/RevModPhys.81.865.

[41] A. S. Holevo, *Probabilistic and statistical aspects of quantum theory*, vol. 1, Springer Science & Business Media (2011).

[42] V. Giovannetti, S. Lloyd and L. Maccone, *Quantum measurement bounds beyond the uncertainty relations*, Phys. Rev. Lett. **108**(26), 260405 (2012).

[43] C. Helstrom and R. Kennedy, *Noncommuting observables in quantum detection and estimation theory*, IEEE Trans. Inf. Theory **20**(1), 16 (1974).

[44] U. Marzolino and T. Prosen, *Quantum metrology with nonequilibrium steady states of quantum spin chains*, Phys. Rev. A **90**, 062130 (2014).

[45] J. Liu, J. Chen, X.-X. Jing and X. Wang, *Quantum fisher information and symmetric logarithmic derivative via anti-commutators*, J. Phys. A: Math. Theor. **49**(27), 275302 (2016), doi:10.1088/1751-8113/49/27/275302.